Low-energy electron scattering from DNA including structural water and base-pair irregularities

Laurent Caron* and Léon Sanche
Groupe de Recherches en Sciences des Radiations, Faculté de médecine, Université de Sherbrooke, Sherbrooke, Québec, Canada J1H 5N4

Stefano Tonzani
Nature Publishing Group, 4 Crinan Street, London N1 9XW, United Kingdom

Chris H. Greene
Department of Physics and JILA, University of Colorado, Boulder, Colorado 80309-0440, USA
(Received 4 May 2009; published 13 July 2009)

Elastic scattering of low-energy (0–13 eV) electrons from more realistic models of a DNA base-pair decamer is studied using multiple-scattering theory and *T* matrices obtained from *ab initio R*-matrix calculations. The models include two types of irregularities usually found in cellular DNA: base-pair mismatch and structural water molecules. Furthermore, we include in our calculation inelastic collisions. It is found that the basic interference patterns observed in the ideal and nonideal (i.e., more realistic) decamers are similar but have different amplitudes and are shifted in energy. Substantial inelastic losses, interestingly, cause pronounced local resonances, which could have an important influence in DNA strand breaks.

DOI: 10.1103/PhysRevA.80.012705 PACS number(s): 34.80.Bm, 87.15.A−, 87.64.Bx

I. INTRODUCTION

In a recent paper [1], henceforth referred to as paper I, low-energy electron elastic scattering from an idealized sequence of ten DNA base pairs was studied. A thrifty multiple-scattering (MS) model was proposed [2–5] which used accurate electron-scattering calculations for the DNA bases obtained using the *R*-matrix method [6,7]. Complex interference modulations were observed in the total wave function, the scattering cross section, and axial currents which emphasized the importance of multiple elastic scattering in electron capture. These results correlated well with experimental data. In this paper, we consider a nonideal decamer in order to evaluate the impact of pair mismatch, structural water molecules, and inelastic losses on the elastic scattering of low-energy electrons that are incident perpendicular to the decamer. It is important to verify, for instance, whether the energy-dependent elastic-scattering features are primarily associated with the structural water molecules surrounding the bases and/or the sugar-phosphate backbone as has been suggested by the recent work of Orlando *et al.* [8].

We first describe the structure of the model decamer and review the theory. Next we explore the effect of pair mismatch, structural H_2O and energy-loss electrons on elastic scattering. All equations are expressed in atomic units (a.u.) in which the Bohr radius is the unit of length and the hartree (2 Ry) is the unit of energy.

II. MODEL

A. Decamer structure

The present study considers the nonideal *B* form of the *GCGAATTGGC* decamer (without backbone) which has two base-pair mismatches: the third base pair from either end is *G*-*G*. This decamer is the inner part of the protein data bank cataloged 1D80 dodecamer 5′-*D*(∗*CP*∗*GP*∗*CP*∗*GP*∗*AP*∗*AP*∗*TP*∗*TP*∗*GP*∗*GP*∗*CP*∗*G*)-3′ [9] with backbone removed and retaining only the 23 innermost water molecules that are in a cylindrical volume contained within 6 a.u. of the outermost tip of the bases and within 6 a.u. of the top and bottom base pairs. A side view of the decamer, plotted with JMOL [10], is shown in Fig. 1.

The structural defects result in a substantial variation in the basic DNA parameters. The regular *B* form of DNA has 10 base pairs per helical turn (thus our choice of a decamer) and hence a 36.0° helical twist, a small tilt (2.8° inclination) relative to the spiral axis but appreciable roll (−15.1° propeller twist) of the base pairs, a rise of 6.39 a.u. between successive base pairs. Our nonideal decamer has an average rise of 6.23 a.u. with a standard deviation of 0.48 a.u. compared to 0.19 for the ideal *GCGAATTGGC* decamer in paper I. As a combined measure of twist and roll, we have taken the polar angle of the normal direction to the bases relative to the spiral direction. The average value here is 0.188 rad with a standard deviation of 0.08 rad compared to 0.11 and 0.0008, respectively, for the ideal decamer. There are thus significant variations in rise, tilt, and roll within our decamer. But let us first review the theoretical framework.

B. Multiple-scattering theory

In paper I, we presented the basic equations for multiple electron scattering within macromolecules, including DNA. For the latter, we proposed a simple model of molecular subunits (i.e., bases, sugars, and phosphates) immersed in an optical potential U_{op}, which is constant between their *R*-matrix shells (or between the muffin tins), a working hypothesis that has been used in the calculations for simple molecules [11], in the theory of low-energy electron diffrac-

*Permanent address: Département de Physique, Université de Sherbrooke, Sherbrooke, Québec, Canada J1K 2R1; laurent-g.caron@usherbrooke.ca

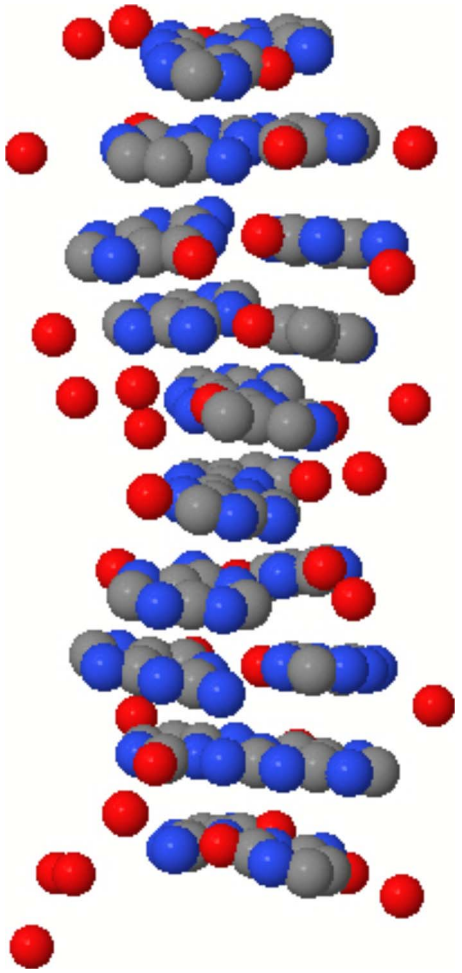

FIG. 1. (Color online) Side view of the decamer. The oxygen atoms of the retained water molecules appear as isolated spheres.

tion (LEED) in solids [12] and nanoscale structures [13]. The only function of the real part of the optical potential is to account for the average energy seen by an electron. One can quite generally describe the scattering problem of a molecular subunit by its scattering matrix $S_{L'L}$ [14,15], where $L=(l,m)$ are the angular momentum quantum numbers. Each molecular subunit has an incident plane wave of momentum $\vec{k}$ impinging on it plus the scattered waves of all other subunits. More specifically, we described the asymptotic form of the total wave function $\psi_{\vec{k}}^{(n)}(\vec{r})$ for a molecule centered at $\vec{R}_n$ outside the R-matrix shell by the following equation:

$$\psi_{\vec{k}}^{(n)}(\vec{r}) = 4\pi e^{i\vec{k}\cdot\vec{R}_n} \sum_{LL'} i^l B_{\vec{k}L}^{(n)} Y_{L'}(\Omega_{\vec{r}_n}) \times \left[j_l(kr_n)\delta_{L'L} + \frac{1}{2}(S_{L'L}^{(n)} - \delta_{L'L}) h_{l'}^{(1)}(kr_n) \right], \quad (1)$$

where Y_L are spherical harmonics, j_l and $h_{l'}^{(1)}$ are the spherical Bessel function and Hankel function of the first kind, respectively, $\vec{r}_n=\vec{r}-\vec{R}_n$, and

$$B_{\vec{k}L}^{(n)} = Y_L^*(\Omega_{\vec{k}}) + \frac{1}{2} \sum_{n'\neq n} \sum_{L_1,L_2,L_2'} i^{l_1+l_2-l_2'} B_{\vec{k}L_2}^{(n')} (S_{L_2'L_2}^{(n')} - \delta_{L_2'L_2}) \times (-1)^{m_2'} e^{-i\vec{k}\cdot\vec{R}_{nn'}} F_{m_1,m,-m_2'}^{l_1,l,l_2'} Y_{L_1}(\Omega_{\vec{R}_{nn'}}) h_{l_1}^{(1)}(kR_{nn'}), \quad (2)$$

where

$$F_{m_1,m,-m_2'}^{l_1,l,l_2'} = [4\pi(2l_1+1)(2l+1)(2l_2'+1)]^{1/2} \begin{pmatrix} l_1 & l & l_2' \\ 0 & 0 & 0 \end{pmatrix} \times \begin{pmatrix} l_1 & l & l_2' \\ m_1 & m & -m_2' \end{pmatrix}$$

and

$$\begin{pmatrix} l_1 & l & l_2' \\ m_1 & m & -m_2' \end{pmatrix}$$

is the Wigner 3-j symbol [16], and $\vec{R}_{nn'}=\vec{R}_n-\vec{R}_{n'}$. Equation (2) implies a coupled set of linear equations for all $B_{\vec{k}L}^{(n)}$, which measure the resultant of the superposition of the incident plane wave and the contribution from all other scatterers. As mentioned before [2,3], the loss of coherence of the electrons due to inelastic collisions can be invoked through an imaginary part in the background optical potential U_{op} [12], i.e., an imaginary part to the electron wave number $\mathrm{Im}(k)=\xi^{-1}$. Here ξ acts as a coherence length for the electrons.

Some nontrivial approximations have had to be attached to these equations to deal with polar molecules. The ground rules for a satisfactory integration were laid in the recent studies of the H_2O molecule in solid ice [17] and the water dimer [18,19]. Fine tuning was achieved in paper I.

(1) A cutoff in the range of action of the dipole must be introduced. We remove the dipole field for $r>a_c$, where a_c is a cut-off radius equal to the R-matrix sphere size in our case.

(2) An upper cutoff must be applied to angular momenta. Only values $l\leq l_o$ should be retained such that $E(l_o,d_m)<E_e<E(l_o+1,d_m)$, where $E(l_o,d_m)=l(l+1)/(2d_m^2)$. We have chosen the value $d_m=11$ a.u. for interbase scattering that is of the order of the size of the bases, the distance between base centers in the base pairs, and the size of the R-matrix sphere so as to retain all of its important energy-dependent characteristics. For the scattering between water molecules and with the bases, we have chosen $d_m=6$ a.u. which is typical of the distance between neighboring water molecules and with neighboring bases.

(3) An interpolation procedure between discrete values of l is used for any scalar quantity. It worked well in I and for the H_2O dimer [18,19]. In the present situation, there are two angular momentum cutoffs, one for bases and one for water that have to be interpolated on.

C. Electron capture and scattering

In an effort to extract physically meaningful information from the multiple-scattering formalism, we have targeted a calculation of the capture amplitude $V_{\vec{k}}^{(n)}$ of an electron in a

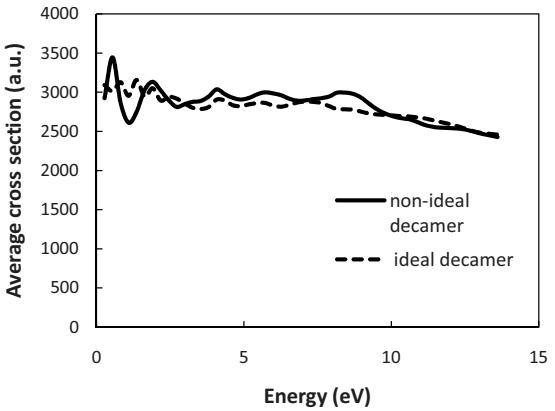

FIG. 2. Elastic cross section of the ideal and nonideal decamers averaged over the two chosen electron incident directions as a function of energy.

shape or core-excited resonance of a basic subunit positioned at $\vec{R}_n$. Assuming a dominant capture channel symmetry corresponding to L_o and using the one-center approximation of O'Malley and Taylor [20], this leads to

$$V_{\vec{k}}^{(n)} = \sqrt{4\pi} V_{l_o} B_{\vec{k}l_o}^{(n)} e^{i\vec{k}\cdot\vec{R}_n}, \tag{3}$$

where V_{l_o} is an energy- and nuclear-coordinate-dependent amplitude. This amplitude contains the dissociative attachment information. There is unfortunately no available theoretical information on the vibrational part of the wave function for the DNA bases at this time. So we shall only focus on the MS part $B_{\vec{k}l_o}^{(n)}$.

We proposed in paper I a weighted partial capture factor

$$\Gamma_w(l_o) = \frac{\sum_{\vec{R}_n} \gamma(l_o, \vec{R}_n)}{\sum_{\vec{R}_n}}, \tag{4}$$

in which the constituent partial capture factor

$$\gamma(l_o, \vec{R}_n) = \frac{\sum_{m_o=-l_0}^{l_0} |\sqrt{4\pi} B_{\vec{k}l_o m_o}^{(n)}|^2}{(2l_0+1)} \tag{5}$$

measures the partial wave decomposition of the total wave function at $\vec{R}_n$ and $\Sigma_{\vec{R}_n}$ is just the total number of subunits. Any dissociative attachment resonance occurring in the l_o channel leads to a capture probability which, by Eq. (3), is modulated by $|B_{\vec{k}l_o}^{(n)}|^2$. $\gamma(l_o, \vec{R}_n)$ can serve as a meaningful measure of the effect of MS on dissociative attachment. Since $\gamma(l_o, \vec{R}_n)=1$ for a lone plane wave, then any value larger than 1 would imply an enhancement of the dissociative attachment resonance cross section due to MS. Note that $\gamma(0, \vec{R}_n)$ equals the absolute square of the wave function at $\vec{R}_n$, and $\Gamma_w(0)$ measures the absolute square of the wave function averaged over all bases.

The total elastic cross section, for a finite-size macromolecule, is also of interest. Technically, we can expand the scattered part of Eq. (1) around the geometric center $\vec{R}_{GC}$ of the macromolecule. In this reference system, remembering that $\vec{r}_n = \vec{r} - \vec{R}_n$, one has

$$\begin{aligned} Y_{L'}(\Omega_{\vec{r}_n}) h_{l'}^{(1)}(kr_n) = \sum_{L_1, L_2} & i^{l_1+l_2-l'} (-1)^{m'} F_{m_1, m_2, -m'}^{l_1, l_2, l'} Y_{L_1}(\Omega_{\vec{r}-\vec{R}_{GC}}) \\ & \times Y_{L_2}(\Omega_{\vec{R}_{GC}-\vec{R}_n}) h_{l_1}^{(1)}(k|\vec{r}-\vec{R}_{GC}|) \\ & \times j_{l_2}(k|\vec{R}_{GC}-\vec{R}_n|). \end{aligned} \tag{6}$$

In the limit $k|\vec{r}-\vec{R}_{GC}|$ large, one can write

$$\lim_{k\rho \ large} h_{l_1}^{(1)}(k\rho) = i^{-l_1-1} e^{ik\rho}/(k\rho), \tag{7}$$

where $\vec{\rho}=\vec{r}-\vec{R}_{GC}$. Therefore, one obtains

$$\begin{aligned} \lim_{k\rho \ large} \psi_{\vec{k}}^{(n)}(\vec{\rho}) = 2\pi \sum_{LL'} & e^{i\vec{k}\cdot\vec{R}_n} i^l B_{\vec{k}L}^{(n)} T_{L'L}^{(n)} \sum_{L_1, L_2} i^{l_1+l_2-l'} \\ & \times (-1)^{m'} F_{m_1, m_2, -m'}^{l_1, l_2, l'} Y_{L_1}(\Omega_{\vec{\rho}}) \\ & \times Y_{L_2}(\Omega_{\vec{R}_{GC}-\vec{R}_n}) j_{l_2} \\ & \times (k|\vec{R}_{GC}-\vec{R}_n|) i^{-l_1-1} e^{ik\rho}/(k\rho), \end{aligned} \tag{8}$$

where

$$T_{L'L}^{(n)} = [S_{L'L}^{(n)} - \delta_{L'L}], \tag{9}$$

is the T matrix. From this, one can calculate the scattered current at distance ρ divided by the incident electron flux. In doing this, one obtains the following definition for the elastic cross section in the lossless situation:

$$\sigma_e(k) = \sum_{L_1} |\phi_{L_1}|^2/|k|^2, \tag{10}$$

$$\begin{aligned} \phi_{L_1} = 2\pi \sum_{nLL'} & e^{i\vec{k}\cdot\vec{R}_n} B_{\vec{k}L}^{(n)} T_{L'L}^{(n)} \sum_{L_2} i^{l+l_2-l'-1} (-1)^{m'} F_{m_1, m_2, -m'}^{l_1, l_2, l'} \\ & \times Y_{L_2}(\Omega_{\vec{R}_{GC}-\vec{R}_n}) j_{l_2}(k|\vec{R}_{GC}-\vec{R}_n|). \end{aligned} \tag{11}$$

D. *R*-matrix calculations

1. Bases

The calculations for the DNA bases were done using the code FERM3D [21], and they are described in detail in Refs. [1,7]. We kept angular momenta up to $l=8$, subject however to the cut-off procedure previously described. We removed the dipole outside the R-matrix sphere of radius 11 a.u. as the very molecules are very closely packed.

2. Water molecules

The T matrices for the water molecule were calculated using the UK molecular R-matrix scattering package [22] as detailed in [18]. Angular momenta up to $l=4$ were kept and the chosen radius of the R-matrix sphere was 6 a.u.. The

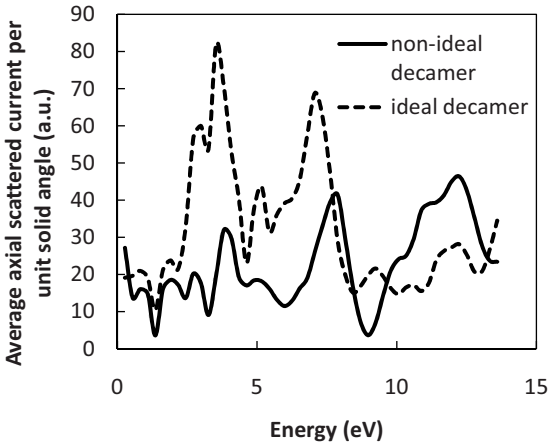

FIG. 3. Axial current of the ideal and nonideal decamers as a function of energy. It is an average over the two chosen electron incident directions and both ± axial exit directions.

electric dipole was removed outside of this sphere.

III. RESULTS AND DISCUSSION

We have chosen to study two mutually orthogonal directions for the incident electron. These are perpendicular to the decamer axis as is the situation in experiments on thin films [23]. They are in plane and out of plane of Fig. 1, perpendicular to the helical axis of the decamer (vertical in figure), as in paper I. We did calculations with 50 different values of the energy in the range 0–13.6 eV.

In paper I we also described the procedure used to transform the T matrices from the R-matrix molecular axes to the actual base position axes within the decamer.

A. Decamer without water molecules

Figure 2 shows the directionally averaged elastic cross section for the nonideal decamer and compares it to the ideal decamer results of paper I. They are very similar except for

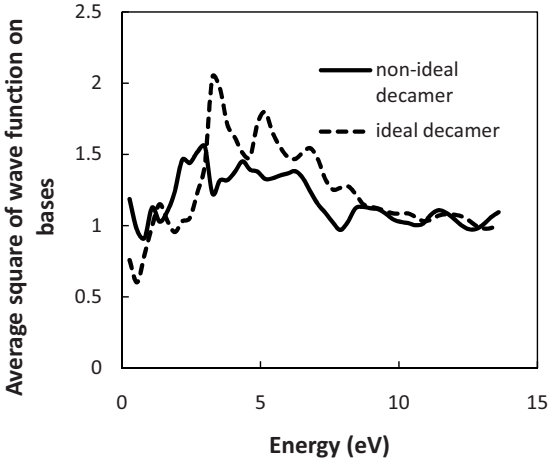

FIG. 4. Base averaged square of the wave function of the ideal and nonideal decamers as a function of energy. It is also averaged over the two chosen electron incident directions.

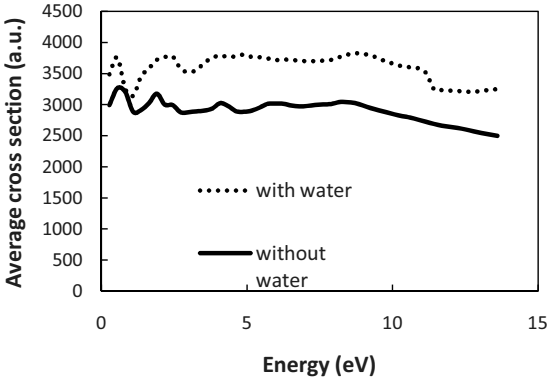

FIG. 5. Elastic cross section of the nonideal decamer with or without the water molecules averaged over the two chosen electron incident directions as a function of energy.

the shift of the 7 eV hump in the ideal decamer to 8 eV in the nonideal one and also around 1 eV where the nonideal curve sinuates strongly. Figure 3 compares the directionally averaged axially scattered current at $\pm\infty$ for the ideal and nonideal decamers, whereas Fig. 4 compares the base averaged square of the wave function at the each base center for the same two decamers. The effect of pair mismatch is seen mostly to decrease the amplitude of the interference patterns below 10 eV in the nonideal decamer in both of these figures. There is a strong accompanying downward energy shift in the case of the square of the wave function. The internal diffraction hump around 11.4 eV discussed in paper I is however increased for the nonideal decamer in both figures. The excess broadening of the internal diffraction peak at 11.4 eV in the axial current might be due to the rather large standard deviation in the rise in the nonideal decamer.

B. Decamer with water molecules

The experimental information available on the position of the water molecules is limited to a knowledge of the position of the oxygen atom of each water molecule with no informa-

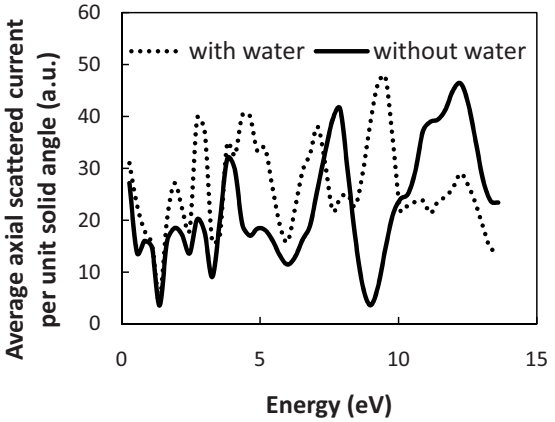

FIG. 6. Contribution of bases to the axial current of the nonideal decamer with or without the water molecules as a function of energy. It is an average over the two chosen electron incident directions and both ± axial exit directions.

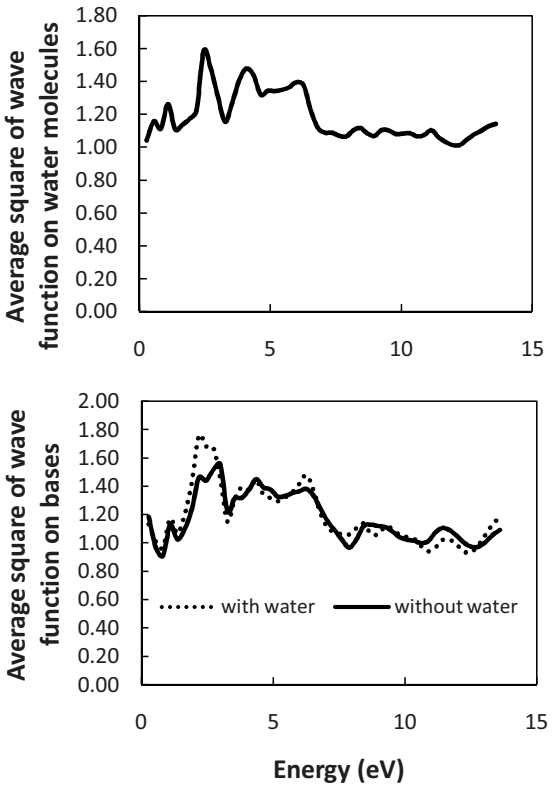

FIG. 7. Square of the electron-scattering wave function as a function of energy: averaged over the water molecules, top part; averaged over the bases, bottom part, compared to the situation without water. It has also been averaged over the two chosen electron incident directions.

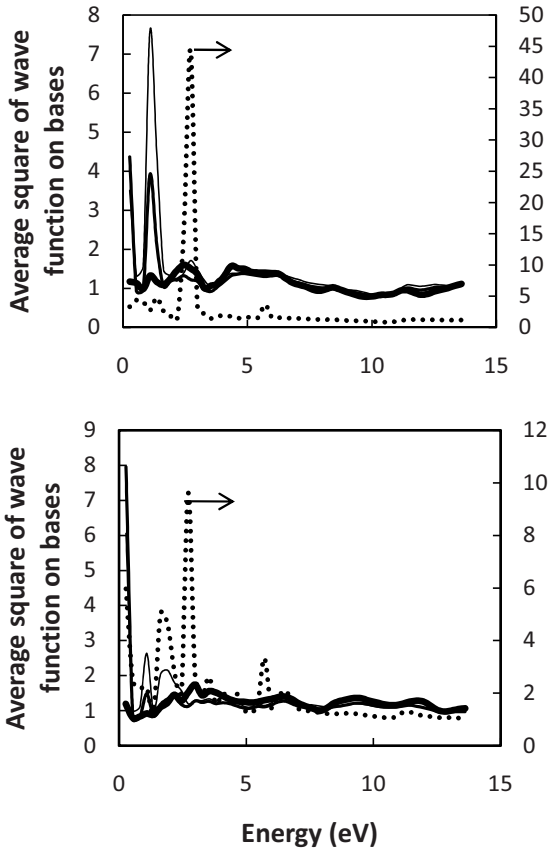

FIG. 8. Base-averaged square of the wave function for an electron scattering from the nonideal decamer for the two chosen incident directions as a function of energy. The chosen values of the coherence length: $\xi=\infty,60,40$ a.u. from thickest to thinnest continuous lines, $\xi=30$ a.u. dotted line (right vertical axis as signaled by arrows).

tion on the position of the hydrogen atoms. We therefore generated a random orientation for each of the water molecules and used the same T-matrix transformation procedure as for the bases. Figure 5 compares the directionally averaged cross section for the decamer with and without water. The difference stems from the contribution of the 23 water molecules which have each an elastic cross section of order of 40 a.u [17]. Figure 6 compares the directionally averaged axially scattered current coming from the bases at $\pm\infty$ for the decamer with and without water. Figure 7 shows the square of the wave function averaged over the water molecules (top part) and averaged over the bases for the same two decamers (bottom part). The interference patterns below 9 eV for the bases are quite similar in both of the latter figures contrary to the findings of Orlando *et al.* [8] which associates features solely to the water molecules. Comparing top to bottom curves of Fig. 7 in the presence of water, one observes that the wave functions on the water molecules are actually base driven. The differences in the results from our model and that of Orlando *et al.* may be related to the considerably different scattering approach, the latter being based on the individual atoms comprising all of the subunits and being limited to first-order scattering. The bases retain their basic interference modulations in the presence of water except for the appearance of a strong peak at 9 eV in the axial current. The only other significant difference is in the axial current above 9 eV where amplitudes change appreciably. The internal diffraction hump at 11.4 eV is quite subdued in Fig. 6 by the presence of the water molecules. This is in line with the Orlando *et al.* predictions. The water molecules scatter the incoming electron in all directions which wash away some of the features arising from normal incidence such as the internal diffraction peak.

C. Decamer with inelastic losses

Inelastic losses lead to the disappearance of electrons from the elastic channel. As mentioned earlier, this loss can be incorporated in our theoretical description by introducing an imaginary part to the electron wave number $\mathrm{Im}(k)=\xi^{-1}$, where ξ is an amplitude coherence length for the electrons.

We have carried out the calculations for three values of the coherence length $\xi=60,40,30$ a.u. which are representative of solids [12,24] and biological materials [25,26]. Figure 8 compares the results for the two incident electron directions: the in-plane and the out-of-plane ones of Fig. 1. The figure shows that strong resonances emerge and they also shift in energy as the coherence length decreases from 40 to 30 a.u. In these main peak resonances, the wavelength of the electron is roughly half of the coherence length. It is also seen that the resonance amplitudes are sensitive to the elec-

tron incoming direction. The resonances involve the adenine bases and the mismatched *G*-*G* pairs to varying degree depending on the resonance. Amplitude decoherence promotes better and stronger correlations between closer neighbor bases due to attenuated influence of farther ones. These resonances could play an important role in strand breaking because they could efficiently funnel electrons to the DNA backbone. In particular, large energy losses to electronic excitation create additional very low-energy electrons ($E < 3$ eV) which, as shown theoretically [27,28] and experimentally [29], have a propensity to transfer to the DNA backbone and break the C-O bond (i.e., break the DNA chain).

IV. CONCLUSIONS

We have seen that interference patterns caused by the bases suffer moderately large amplitude modulations and energy shifts in the presence of pair mismatch or water molecules. They, however, retain most of their attributes. Amplitude decoherence, in contrast, singles out large resonances that are sensitive to the incident electron direction. These resonances shift in energy as the coherence length gets small. They may efficiently transfer electrons to the backbone and lead to dissociation.

ACKNOWLEDGMENTS

S.T. was supported by NSF and NSEC and L.S. by CIHR and NSERC. The work of C.H.G. was supported partly by an allocation of NERSC supercomputing resources that were used to perform the *R*-matrix calculations, and in part by the (U.S.) Department of Energy, Office of Science. We thank D. Bouchiha for providing the *T* matrices for the water molecules.

[1] L. Caron, L. Sanche, S. Tonzani, and C. H. Greene, Phys. Rev. A **78**, 042710 (2008).
[2] L. G. Caron and L. Sanche, Phys. Rev. Lett. **91**, 113201 (2003).
[3] L. Caron and L. Sanche, Phys. Rev. A **70**, 032719 (2004).
[4] L. Caron and L. Sanche, Phys. Rev. A **72**, 032726 (2005).
[5] L. Caron and L. Sanche, Phys. Rev. A **73**, 062707 (2006).
[6] S. Tonzani and C. H. Greene, J. Chem. Phys. **122**, 014111 (2005).
[7] S. Tonzani and C. H. Greene, J. Chem. Phys. **124**, 054312 (2006).
[8] T. M. Orlando, D. Oh, Y. Chen, and A. B. Aleksandrov, J. Chem. Phys. **128**, 195102 (2008).
[9] Can be found in the Nucleic Acid Database at http://ndbserver.rutgers.edu/ and the Protein Data Base at http://www.pdb.org/pdb/home/home.do
[10] JMOL: an open-source Java viewer for chemical structures in three-dimensional (3D) http://www.jmol.org/
[11] D. Dill and J. L. Dehmer, J. Chem. Phys. **61**, 692 (1974).
[12] J. B. Pendry, *Low Energy Electron Diffraction* (Academic, London, 1974).
[13] G. A. Fiete and E. J. Heller, Rev. Mod. Phys. **75**, 933 (2003).
[14] N. F. Mott and H. S. W. Massey, *The Theory of Atomic Collisions*, 3rd ed. (Clarendon, Oxford, 1965).
[15] F. A. Gianturco and A. Jain, Phys. Rep. **143**, 347 (1986).
[16] A. Messiah, *Quantum Mechanics* (Wiley, New York, 1962), Appendix C.
[17] L. Caron, D. Bouchiha, J. D. Gorfinkiel, and L. Sanche, Phys. Rev. A **76**, 032716 (2007).
[18] D. Bouchiha, L. G. Caron, J. D. Gorfinkiel, and L. Sanche, J. Phys. B **41**, 045204 (2008).
[19] S. Caprasecca, J. D. Gorfinkiel, D. Bouchiha, and L. G. Caron, J. Phys. B **42**, 095205 (2009).
[20] T. F. O'Malley and H. S. Taylor, Phys. Rev. **176**, 207 (1968).
[21] S. Tonzani, Comput. Phys. Commun. **176**, 146 (2007).
[22] Information can be found at http://www.tampa.phys.ucl.ac.uk/rmat/
[23] L. Sanche, in *Radiation Induced Molecular Phenomena in Nucleic Acid: A Comprehensive Theoretical and Experimental Analysis*, edited by J. Leszczynski (Springer, New York, 2008), Chap. 19.
[24] M. Michaud, L. Sanche, C. Gaubert, and R. Baudoing, Surf. Sci. **205**, 447 (1988).
[25] B. Boudaïffa, P. Cloutier, D. Hunting, M. A. Huels, and L. Sanche, Radiat. Res. **157**, 227 (2002).
[26] Z. Cai, M.-E. Dextraze, P. Cloutier, D. Hunting, and L. Sanche, J. Chem. Phys. **124**, 024705 (2006).
[27] R. Barrios, P. Skurski, and J. Simons, J. Phys. Chem. B **106**, 7991 (2002).
[28] J. Berdys, I. Anusiewicz, P. Skurski, and J. Simons, J. Am. Chem. Soc. **126**, 6441 (2004).
[29] F. Martin, P. D. Burrow, Z. Cai, P. Cloutier, D. Hunting, and L. Sanche, Phys. Rev. Lett. **93**, 068101 (2004).